ELSEVIER

Journal of Analytical and Applied Pyrolysis
42 (1997) 123–133

JOURNAL of ANALYTICAL and APPLIED PYROLYSIS

Texture and morphology of titania particles prepared by vapor-phase pyrolysis of titanium tetra-isopropoxide

Kamal M.S. Khalil [a], Mohamed I. Zaki [b,*], Ahmed A. El-Samahy [a]

[a] *Chemistry Department, Faculty of Science, South-of-Valley University, Sohag 82524, Egypt*
[b] *Chemistry Department, Faculty of Science, University of Kuwait, P.O. Box 5969, Safat 13060, Kuwait*

Received 6 November 1996; accepted 28 January 1997

Abstract

$Ti(OPr^i)_4$ vapor was pyrolyzed in dry nitrogen atmosphere using a simple tubular flow reactor at 400 and 800°C. Well-defined spheroidal anatase TiO_2 particles showing mesoporous surfaces of 30 $m^2\ g^{-1}$ and assuming two different morphologies (fused and composite) were produced at the low temperature (ca. 400°C), whereas deformed spheroidal particles of rutile-structured TiO_2 and surfaces of 12 $m^2\ g^{-1}$ were obtained at the high temperature (ca. 800°C). Particles of the high-temperature product were distinguished by a low porosity and a uniform morphology (composite). The heat-induced modifications at 800°C may be ascribed to enhancements in (a) hydrolysis of $Ti(OPr^i)_4$, by a possible generation of water vapor as a secondary pyrolysis product of the alkoxide, (b) particle growth via coalescence rather than by vapor deposition, and (c) particle sintering. The pyrolysis products were characterized by X-ray diffractometry, high-resolution transmission electron microscopy, and volumetry of nitrogen adsorption at liquid nitrogen temperature.

Keywords: Pyrolysis; Titanium tetra-isopropoxide; Titania; Surface texture; Particle morphology

1. Introduction

Titania, TiO_2, is an industrially and technologically important material, and is widely applied as a pigment, catalyst, and photo-conductor [1]. It is advantageous in these applications to employ titania powders consisting of spheroidal particles of

* Corresponding author.

PII S0165-2370(97)00023-5

submicron sizes [1]. Spheroidal TiO_2 particles with a modal diameter in the range from 1 to 4 nm are obtained by hydrolysis, at elevated temperatures, of highly acidic solutions of $TiCl_4$ in the presence of sulfate ions [2]. However, the procedure is time-consuming and gives very low yields [2]. Hydrolysis of titanium tetra-ethoxide aerosols yields TiO_2 spheroids of a broad size distribution (60–600 nm) [1]. Titanium tetrachloride is also used as a liquid aerosol material; however, the resulting TiO_2 powder consists of spheres of an even broader size distribution [1]. Submicron, highly porous TiO_2 powders ($S_{BET} \sim 320$ m^2 g^{-1}) have been synthesized by vapor-phase hydrolysis of titanium tetra-isopropoxide, $Ti(OPr^i)_4$, in a tubular flow-reactor (under atmospheric pressure) at 150–490°C [3,4]. The particle size was found to increase with increasing inlet $Ti(OPr^i)_4$ concentration and decreasing inlet H_2O concentration and temperature. Ultrafine TiO_2 particles are prepared by vapor-phase deposition of $Ti(OPr^i)_4$ [5,6]. The reaction takes place at a temperature as low as 250°C to give amorphous, porous TiO_2 of a specific surface area of 300 m^2 g^{-1}.

The present investigation was designed to characterize TiO_2 particles obtained by vapor-phase pyrolysis of $Ti(OPr^i)_4$ at elevated temperatures (400 and 800°C) in a dry atmosphere of N_2. X-ray powder diffractometry (XRD), N_2 gas adsorption at liquid nitrogen temperature, and transmission electron microscopy (TEM) were the characterization techniques.

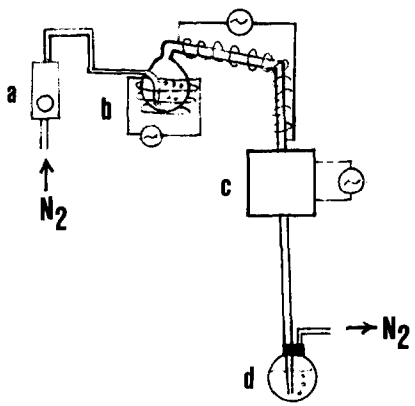

Fig. 1. The pyrolysis system: (a) N_2 gas pressure and flow controller, (b) $Ti(OPr^i)_4$ vaporizer kept at 100°C, (c) a highly conducting tubular furnace housing a quartz tubular reactor (20 cm long; 1 cm wide), and (d) a Pyrex glass receiver containing distilled water.

2. Experimental

2.1. Vapor-phase pyrolysis

The pyrolysis system is shown in Fig. 1. Titanium isopropoxide, $Ti(OPr^i)_4$, held in the vaporizer (b) at 100°C, was transported in the vapor phase by a controlled stream of (a) dry nitrogen (1.0 l min^{-1}) into the 20 cm long hot zone of a quartz tubular reactor (c). The temperature was adjusted to either 400 or 800 ± 2°C to obtain, respectively the two solid materials denoted below as A and B. The carrier gas was vented through liquid water (d) in order to trap the material particles. The suspended particles were then separated by filtration. At 400°C some of the resulting particles were deposited on the reactor inner walls, particularly in the lower half. Some carbonaceous material was also deposited (at 400°C) just beneath the hot zone of the reactor. At 800°C, however, the amount of wall deposition was negligible; no carbonaceous material was observed. Finally, the collected particles, which were poorly crystallized, were dried and further calcined (in air) for 1 h at each respective preparation temperature (i.e. at 400°C for 'A' and at 800°C for 'B'), using a muffle furnace. The calcination products, which were finely divided white powders, were subjected to characterization.

2.2. Characterization techniques

X-ray diffractometry (XRD) was carried out using a model JSX-60 PA Jeol diffractometer (Japan), equipped with a source of Ni-filtered Cu Kα radiation ($\lambda = 0.15405$ nm). The diffractometer was operated at 40 kV and 30 mA, and the diffractograms were recorded at 2θ between 10–80°. Diffraction patterns were matched with ASTM standards [7], for crystalline phase identification purposes.

Nitrogen gas adsorption isotherms were determined on test materials at liquid nitrogen temperature (− 195°C), using a conventional volumetric method [8]. Test materials were outgassed at 100°C for 2 h and cooled to liquid nitrogen temperature prior to exposure to the nitrogen adsorptive. The surface area ($m^2\ g^{-1}$) was determined by BET-analysis [9] of the resulting isotherms. Pore volume calculations were carried out using input data derived from the adsorption branch of the isotherms [10].

Transmission electron microscopy (TEM) was performed using a model JEM-1010 Jeol instrument (Japan). Test samples were prepared by dispersing the solid particles ultrasonically in water, and a drop of the resulting suspension was doped onto a carbon-coated grid and allowed to dry at 60°C. Several grids were prepared for each sample by this method and investigated by TEM at 100 kV.

3. Results

3.1. X-Ray powder diffractograms

Fig. 2 shows XRD patterns for the $Ti(OPr^i)_4$ pyrolysis products A (at 400°C) and B (at 800°C). Values of the d-spacing determined for the product A (Fig. 2) match

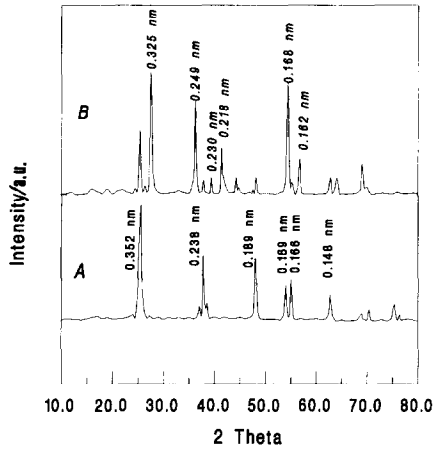

Fig. 2. X-Ray powder diffractograms (Cu Kα radiation) for $Ti(OPr^i)_4$ pyrolysis products A, at 400°C, and B, at 800°C.

well with the standard values [7] for anatase TiO_2 (Table 1). Accordingly, product A can be identified as pure anatase-structured TiO_2. For the product B, d-spacing values for the strongest diffraction peaks (indicated in italics) match well with the standard d-spacings for rutile TiO_2 (Table 1). The weak peaks, also observed for the product B, are due to a minor proportion of anatase TiO_2 (Fig. 2Table 1). Thus, the $Ti(OPr^i)_4$ pyrolysis at 800°C produces a material (B) consisting essentially of rutile TiO_2 with a minor proportion of anatase TiO_2.

Table 1
A comparison between XRD-determined *d*-values (in nm) for pyrolysis products (A) and (B) and those reported [7] for standard titanias

Experimental		ASTM [7]			
Product A	Product B	Anatase TiO_2		Rutile TiO_2	
d-Values	*d*-Values	*d*-Values	(*hkl*)	*d*-Values	(*hkl*)
0.352	0.352	0.352	101		
	0.325			0.325	110
	0.249			0.249	101
0.238	0.237	0.238	004		
	0.230			0.230	200
	0.218			0.219	111
0.189		0.189	200		
0.169		0.170	105		
	0.168			0.169	211
0.166		0.167	211		
	0.162			0.162	220
0.148		0.148	204		

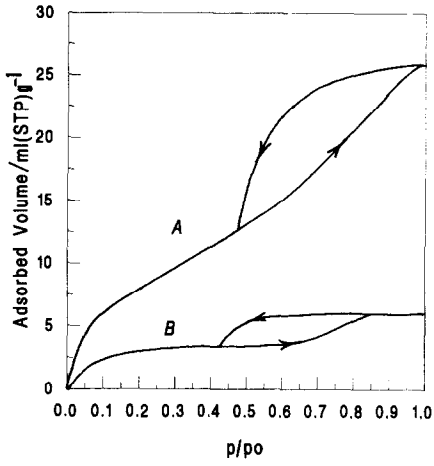

Fig. 3. N_2 adsorption/desorption isotherms determined (at liquid nitrogen temperature) on the pyrolysis products (A) and (B).

3.2. Nitrogen adsorption isotherms

Fig. 3 shows nitrogen adsorption/desorption isotherms determined on the $Ti(O\text{-}Pr^i)_4$ pyrolysis products (A) and (B). According to Brunauer et al. [11], the two isotherms are of type IV, and the displayed hysteresis loops are of type H2 [12]. Hence, both pyrolysis products exibit porous surfaces, and the pores are ink-bottle-like, forming a 'network' structure [12]. The amounts of N_2 at $p/p_0 = 1.0$ (Fig. 3) account for a much larger total pore volume for product A (namely, 0.03 ml g^{-1}; see [12] for calculations) than B (0.006 ml g^{-1}). BET-analysis of the isotherms consistently showed a higher specific surface area for product A (30 m^2 g^{-1}) than B (12 m^2 g^{-1}). The well-defined 'knee' displayed in the isotherm of product A at $p/p_0 < 0.1$, as compared to the ill-defined knee exhibited in the isotherm of product B, implies stronger adsorbent-adsorbate interactions with product A.

Pore volume distribution curves (dv/drp vs. $r\bar{p}$) constructed for the pyrolysis products are shown in Fig. 4. The results indicate that most of the large total pore volume determined for product A is due essentially to narrow mesopores ($r\bar{p} = 1.5$–2.0 nm). The results also show that the notable drop in the total pore volume of product B is attributable to the observed elimination of porosity in the narrow pore radius range. The low porosity observed for product B is due essentially to wide mesopores ($r\bar{p} = 3.0$–4.0 nm).

3.3. TEM micrographs

Fig. 5 shows TEM micrographs obtained for the pyrolysis products (A) and (B). The top micrograph indicates that product A consists of spheroidal particles, some of which are fused together. Weak-ring electron diffraction patterns characteristic of anatase TiO_2 were exhibited by the particles. Spotty patterns were never obtained

for any of the particles. These results indicate that single crystals of anatase TiO_2 were not formed under the experimental conditions for product A. The bottom micrograph (Fig. 5) (for product B) shows highly deformed spheroidal particles, many of which gave rise to a spotty electron diffraction pattern typical of single crystals of rutile TiO_2.

Particle size distribution graphs (Fig. 6) were constructed for the two products (A) and (B), by measuring the sizes of more than 700 particles observed in TEM micrographs. The results indicate that the particle size of product A ranges between 50–400 nm, with the maximum at 150 nm. On the other hand, the particle size of product B is shown (Fig. 6) to range between 50–250 nm, with the maximum at 100 nm. The results thus indicate that the size distribution of the particles narrows and shifts towards smaller values upon increasing the pyrolysis temperature from 400 to 800°C.

High resolution transmission electron micrographs (HRTEM) obtained for the two materials (A) and (B) are displayed in Fig. 7. The top micrograph reveals two different particle morphologies for the product A: fused particles of low porosity, see *x* and *y*; and composite mesoporous particles consisting of a collection of many tiny particles, see *z*. The size of mesopores observed ranges between 2 and 20 nm. The bottom HRTEM micrograph (Fig. 7) shows that the deformed spheroidal particles comprising the product B are dominated by micropores of sizes largely below 2 nm. Thus, the failure of N_2 adsorption to detect narrow mesopores in the product B (Fig. 4) may be attributed to the presence of pores too small to admit N_2 molecules (cross sectional area per N_2 molecule = 16.2 $Å^2$ [12]).

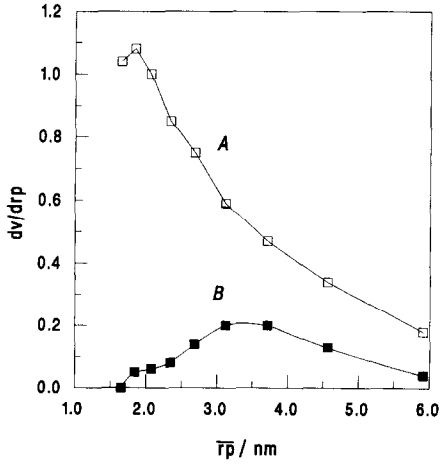

Fig. 4. Pore volume distribution (dv/drp) vs. mean pore radius (rp) curves derived from the adsorption branch of each respective isotherm for the products (A) and (B).

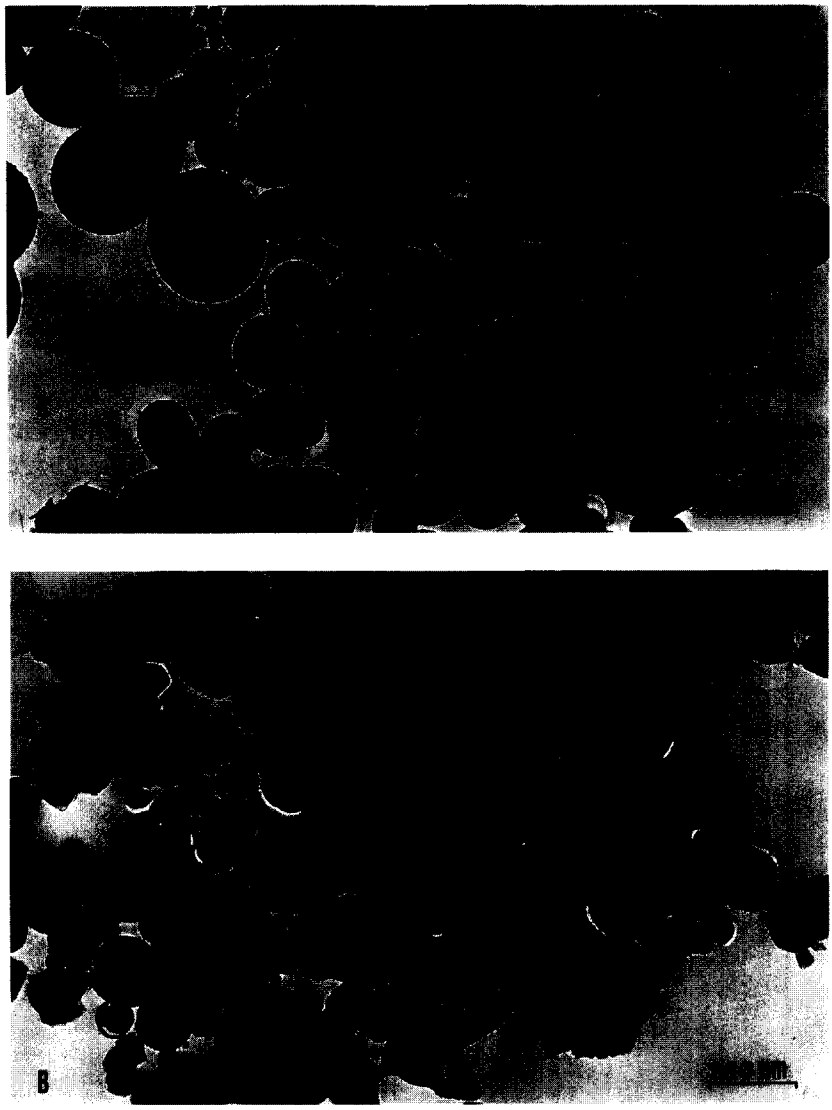

Fig. 5. TEM micrographs for the pyrolysis product A and B obtained at the magnifications indicated.

4. Discussion

4.1. $Ti(OPr^i)_4$ pyrolysis

Literature reports indicate that the pyrolysis of $Ti(OPr^i)_4$ commences near 250°C and proceeds in accordance with the following reaction [5],

$$Ti(OPr^i)_4\ \text{Vapour} \rightarrow TiO_2 \cdot nH_2O\downarrow + 4C_3H_6\uparrow + (2-n)H_2O\uparrow \quad (1)$$

Formation of C_3H_6 and H_2O in the reaction products has been attributed to a catalytic dehydration of isopropanol (a primary pyrolysis product) on the freshly generated surfaces of titanium dioxide [3], according to the following reaction:

$$C_3H_7OH \rightarrow C_3H_6 + H_2O \quad (2)$$

Dehydration of isopropanol on TiO_2 has been found to occur quantitatively (i.e. 100% conversion) at 415°C [13]. The presence of H_2O vapor in the pyrolysis atmosphere makes possible a simultaneous hydrolysis of $Ti(OPr^i)_4$ [4], which is readily activated above 110°C:

$$Ti(OPr^i)_4 + (2+n)H_2O \rightarrow TiO_2 \cdot nH_2O\downarrow + 4Pr^iOH\uparrow \quad (3)$$

Except for the initial pyrolysis period of $Ti(OPr^i)_4$, both reaction mechanisms (Eq. (1)) and (Eq. (3)) are likely to occur simultaneously under the present experimental conditions.

4.2. Product particle formation

Particle formation and growth for solid products of vapor phase pyrolysis are reported to involve five basic steps [3]: (1) chemical reaction, (2) particle nucleation, (3) particle growth by vapor deposition either as a result of chemical reaction or physical condensation, (4) particle collision, and (5) particle growth by coalescence.

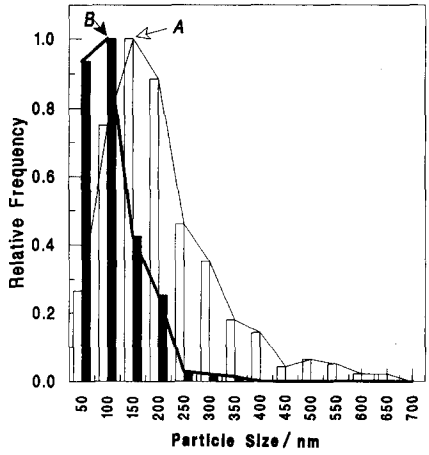

Fig. 6. Particle size distribution graphs as derived from TEM micrographs of the pyrolysis products (A) and (B).

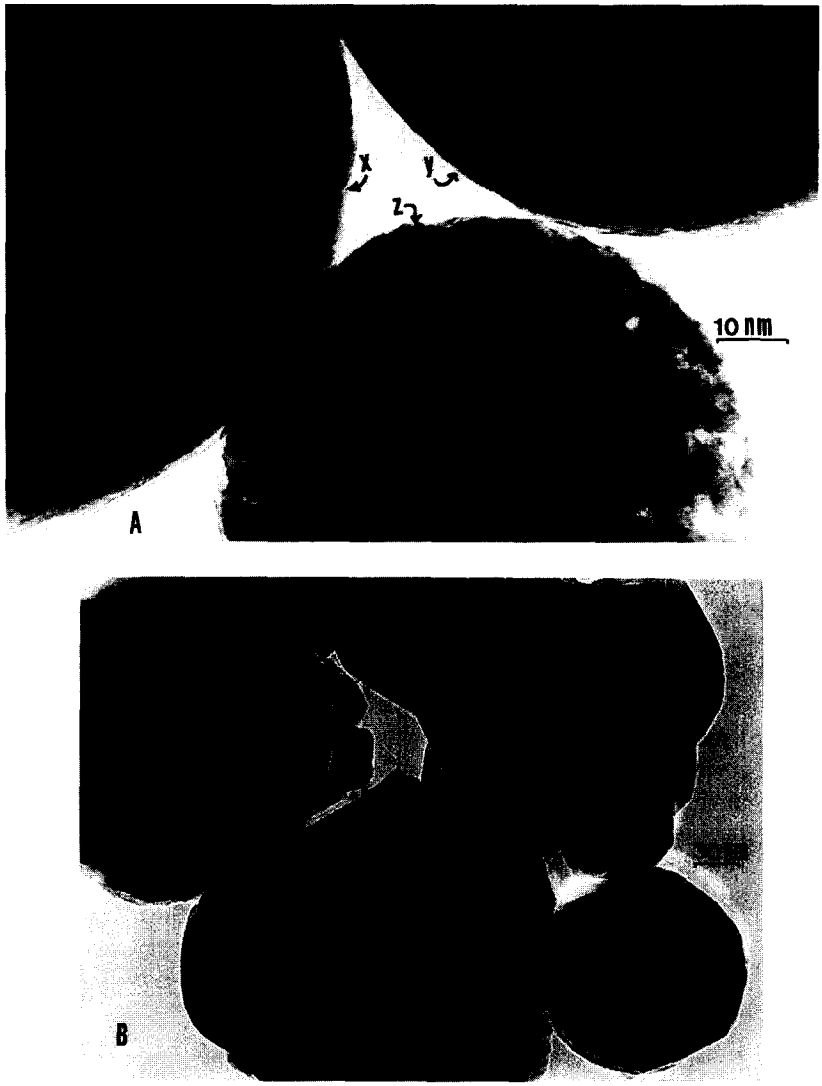

Fig. 7. HRTEM micrographs for the pyrolysis products (A) and (B) obtained at the magnifications indicated.

The TEM observation (Fig. 5) of well-defined spheroidal particles of two different morphologies (fused and composite, Fig. 7) in the material of product A indicates the predominance at 400°C of the pyrolysis over the hydrolysis reaction of $Ti(OPr^i)_4$. This also favors particle growth via vapor deposition (step 3) over growth by coalescence (step 5). The dominance of the composite particle morphology in product B may imply that (at the higher temperature of 800°C) the

hydrolysis of the alkoxide and the particle growth by coalescence are enhanced so that they surpass the competing alternatives.

4.3. Product texture and morphology

It has been reported [6] that porous particles of non-crystalline TiO_2 produced by chemical vapor deposition are stable at $\leq 250°C$. Above that temperature crystallization occurs to yield anatase TiO_2, however maintaining the porous texture. Above 390°C, the particles are sintered to assume non-porous surfaces [6]. Our results agree with the above reported data, as they indicate formation of fused and composite, well defined spheroidal particles (TEM, Figs. 5 and 7) of anatase-structured TiO_2 (XRD, Fig. 2). These possess N_2-accessible narrow porous surfaces of 30 $m^2\ g^{-1}$ (Figs. 3 and 4). The particle size ranges essentially between 5 and 400 nm, with maximum near 150 nm (Fig. 6). At 800°C, the anatase structure is converted (incompletely), into the rutile modification (Fig. 2), the spheroidal particles are deformed (Fig. 5) and become dominantly of a composite morphology rather than a fused one (Fig. 7), and surfaces have a poor specific area (12 $m^2\ g^{-1}$) with a N_2-inaccessible microporosity (Fig. 4). The particle size distribution (Fig. 6) indicates a concomitant decrease in the average particle diameter to maximize near 100 nm, instead of 150 nm for the low-temperature product.

The above heat-inducted textural and morphological modifications may be correlated to consequent enhancements in the following processes: (a) hydrolysis of $Ti(OPr^i)_4$, utilizing water vapor generated as a secondary pyrolysis product of the alkoxide, (b) particle growth via coalescence, and (c) particle sintering. It is worth noting that particle sintering normally results in the narrowing of surface pores and an increase in the particle size. In contrast, the average particle size of the present rutile TiO_2 (produced at 800°C) is shown (Fig. 6) to be less than that of the anatase TiO_2 (produced at 400°C). This unexpected behavior may be due to the re-crystallization of the product, viz. anatase $\rightarrow$ rutile TiO_2, at $> 400°C$.

References

[1] M. Visco, E. Matijevic, J. Colloid Interface Sci. 68 (1979) 308.
[2] E. Matijevic, M. Budink, L. Meites, J. Colloid Interface Sci. 61 (1977) 308.
[3] F. Kirkbir, H. Komiyama, Adv. Ceram. Mater. 3 (1988) 511.
[4] F. Kirkbir, H. Komiyama, Chem. Soc. Jpn. Chem. Lett. 5 (1988) 791.
[5] H. Komiyama, T. Kanai, H. Inoue, Chem. Soc. Jpn. Chem. Lett. 8 (1984) 1283.
[6] K. Morishige, F. Kanno, S. Ogawara, S. Sasaki, J. Phys. Chem. 89 (1985) 4404.
[7] X-Ray Powder Data Files, American Society for Testing and Materials (ASTM), J.V. Smith. (Ed.), Philadelphia, USA, 1960.
[8] S.J. Gregg, K.S.W. Sing, Adsorption, Surface Area and Porosity, Academic Press, London, 1967, pp. 308–316.
[9] S.J. Gregg, K.S.W. Sing, Adsorption, Surface Area and Porosity, Academic Press, London, 1967, pp. 36-44.
[10] C. Orr, J.M. Dalla Valle, Fine Particles Measurement, MacMillan, New York, 1959, pp. 271.
[11] S. Brunauer, P.H. Emmett, E. Teller, J. Am. Chem. Soc. 60 (1938) 309.

[12] A.J. Lecloux, in: J.R. Anderson, M. Boudart (Eds.), Catalysis: Science and Technology, Springer-Verlag, Berlin, 1981, pp. 171.
[13] I. Carrizosa, G. Munuera, J. Catal. 49 (1977) 174–189.